

RESEARCH

Open Access



# ETV4/ALYREF-mediated glycolytic metabolism through PKM2 enhances resistance to ferroptosis and promotes the development of intrahepatic cholangiocarcinoma

Xiaohui Wang<sup>1</sup>, Wenbin Duan<sup>1</sup>, Zhongzhi Ma<sup>1</sup>, Haoquan Wen<sup>1</sup>, Xianhai Mao<sup>1,2</sup> and Changjun Liu<sup>1\*</sup>

## Abstract

**Background** Intrahepatic cholangiocarcinoma (ICC) is the second most common primary hepatocellular cancer. This study investigated whether *ETV4*, *ALYREF*, and *PKM2* affect glycolytic metabolism and ferroptosis, thereby potentially influencing ICC.

**Methods** Bioinformatic analysis was used to explore the expression levels and prognosis of *ETV4*, *ALYREF*, and *PKM2* in ICC and their regulatory relationships were confirmed using in vitro experiments. Glycolytic metabolism and ferroptosis were examined, and chromatin immunoprecipitation and RNA immunoprecipitation experiments were performed to verify whether the *ETV4*, *PKM2*, and *ALYREF* could bind. The effect of *ETV4/ALYREF* on ICC was further confirmed by in vivo experiments.

**Results** *ETV4*, *ALYREF*, and *PKM2* were highly expressed in ICC. Overexpressed (oe)-*ETV4* and oe-*PKM2* promoted cell migration and increased glucose (GLU) utilization and lactate and intracellular adenosine triphosphate (ATP) production. Addition of the ferroptosis inducer Erastin to the above groups revealed that sh-*ETV4* and sh-*ALYREF* increased lipid reactive oxygen species (ROS), malondialdehyde (MDA), and Fe<sup>2+</sup> levels, and oe-*PKM2* reversed these effects in the sh-*ETV4* and sh-*ALYREF* groups. Oe-*ETV4* promoted the expression of *PKM2*, whereas sh-*ALYREF* inhibited the same. *ETV4* could bind to *ALYREF* and *PKM2* promoter, and *ALYREF* could promote the stability of *PKM2* in an m5C-dependent manner. In vivo, *ETV4* promotes tumor growth and the expression of proteins related to glycolytic metabolism by regulating *ALYREF*.

**Conclusion** *ETV4* promotes ICC development and ferroptosis resistance by facilitating glycolytic metabolism, and regulating *PKM2* transcription by directly binding to the *PKM2* promoter. Additionally, it mediates m5C-dependent *PKM2* stabilization by directly binding to *ALYREF*. This study identified a new potential therapeutic target for ICC.

**Keywords** ICC, *PKM2*, *ETV4*, *ALYREF*, Glycolytic metabolism, Ferroptosis, m5C

\*Correspondence:

Changjun Liu  
liuchangjun712@163.com

<sup>1</sup>Department of Hepatobiliary Surgery, Hunan Provincial People's Hospital, The First Affiliated Hospital of Hunan Normal University, No. 61, Jiefang West Road, Furong District, Changsha 410000, Hunan, China

<sup>2</sup>Department of Hepatobiliary and Intestinal Surgery, Hunan Cancer Hospital and the Affiliated Cancer Hospital of Xiangya School of Medicine, Central South University, 410013 Changsha, China



© The Author(s) 2025. **Open Access** This article is licensed under a Creative Commons Attribution-NonCommercial-NoDerivatives 4.0 International License, which permits any non-commercial use, sharing, distribution and reproduction in any medium or format, as long as you give appropriate credit to the original author(s) and the source, provide a link to the Creative Commons licence, and indicate if you modified the licensed material. You do not have permission under this licence to share adapted material derived from this article or parts of it. The images or other third party material in this article are included in the article's Creative Commons licence, unless indicated otherwise in a credit line to the material. If material is not included in the article's Creative Commons licence and your intended use is not permitted by statutory regulation or exceeds the permitted use, you will need to obtain permission directly from the copyright holder. To view a copy of this licence, visit <http://creativecommons.org/licenses/by-nc-nd/4.0/>.

## Introduction

Cholangiocarcinoma (CCA) is a primary malignant tumor that is classified into two types, i.e., intrahepatic and extrahepatic [1]. Intrahepatic cholangiocarcinoma (ICC) is the second most common primary hepatic carcinoma with an increasing incidence rate [2]. It originates from the epithelial cells of the intrahepatic bile ducts and typically presents no symptoms in its early stages. ICC is frequently diagnosed in advanced stages, contributing to a low survival rate [3–5]. The treatment modalities for ICC include targeted therapy, immunotherapy, and surgical intervention [6]. Among these, surgery remains the primary treatment method for ICC; this is especially concerning because ICC is associated with a poor prognosis and a high recurrence rate [6, 7]. Only a small proportion of the patients are eligible for the operation [5]. Therefore, identifying novel therapeutic targets that can prolong the survival of patients with ICC is crucial.

One of the most common biochemical characteristics of cancer cells is aberrant metabolism of glucose (GLU), with glycolysis being the first step in GLU degradation [1, 8]. Cancer cells have a vigorous glycolytic pathway that produces lactate (LD) and adenosine triphosphate (ATP) [8, 9]. LD also promotes cancer development [8, 9]. Pyruvate kinase M2 (PKM2), a key enzyme in glycolysis, is highly expressed in ICC, resulting in unfavorable outcomes [10]. In bladder cancer, HIF-1 $\alpha$  can indirectly upregulate PKM2 by activating Aly/REF nuclear export factor (ALYREF), thereby promoting GLU metabolism [11]. ALYREF is a nuclear RNA-binding protein that recognizes and binds 5-methylcytosine (m5C) [12]. High ALYREF levels promote the development of bladder cancer and hepatocellular carcinoma [11, 13]. However, the regulatory relationship between ALYREF and PKM2 in the ICC remains unclear.

Ferroptosis, an area of focus in cancer therapy, is an iron-dependent form of cell death that is distinct in terms of morphology and genetics from other types of regulatory cell death [14]. It occurs through both exogenous and transporter protein-dependent pathways as well as through endogenous or enzyme regulation pathways [15]. Ferroptosis is characterized by the production of reactive oxygen species (ROS) and accumulation of lipid peroxides and iron [16–18]. It is crucial for maintaining balance within the body, and its dysregulation has been shown to play a critical role in cancer [19]. Previous studies have demonstrated that PKM2 suppresses ferroptosis in pancreatic cancer [20]. Therefore, we hypothesized that ALYREF and PKM2 are involved in glycolytic metabolism and ferroptosis in ICC.

E26 transformation-specific variant 4 (ETV4), a member of the polyomavirus enhancer activator 3 (PEA3) subfamily, is activated in various types of cancers [21, 22]. Enhanced ETV4 expression promotes

cholangiocarcinoma cell proliferation and invasiveness [23].  $\alpha$ -Ketoglutarate has the potential to enhance ETV4 expression and prevent iron-induced cell death [24]. Moreover, our prediction using the JASPAR database suggests that ETV4 might bind to the ALYREF/PKM2 promoter. Therefore, we postulated that the ETV4/ALYREF/PKM2 axis may have an impact on ICC progression and could potentially exert influence through glycolytic metabolism and ferroptosis.

## Materials and methods

### Cell lines

Human intrahepatic cholangiocarcinoma cells (HCCC-9810; AW-CCH049; Abiowell, China) and human intrahepatic cholangiocarcinoma cells (RBE cells; iCell-h265; iCell, China) were cultured in RPMI-1640 medium (iCell-0002; iCell) supplemented with 10% fetal bovine serum (FBS; 10099141; Gibco, USA) and dual antibodies (AWH0529a; Abiowell). The cells were then incubated at 37 °C in an atmosphere of 5% CO<sub>2</sub>.

### Cell transfection

The synthetic shRNA plasmids targeting ETV4, ALYREF, and NSUN2, overexpression plasmids for ETV4, ALYREF, and PKM2, and their respective negative controls (NC) were obtained from HonorGene, Shanghai, China. Following the manufacturer's instructions, plasmids were transfected separately into HCCC-9810 and RBE cells using Lipofectamine 2000 (11668500; Invitrogen, USA).

### Western blotting (WB)

The expression of ETV4, PKM2, ALYREF, PDK1, LDHA, GLUT1, and NSUN2 in HCCC-9810 and RBE cells, as well as in subcutaneous xenografts, was detected using WB. Total protein from cells and xenografts was extracted using RIPA lysis buffer (CW2333S; CWBIO, China), and the protein concentration was determined using a BCA assay kit (P0010S; Beyotime, China). Subsequently, the proteins were separated by SDS-PAGE, transferred onto nitrocellulose (NC) membranes (IB23001; Invitrogen), and then incubated with primary and secondary antibodies at room temperature. After washing with TBST, the membranes were incubated with an ECL Plus ultrasensitive chemiluminescence substrate (K-12045-D50; Advantisa, Japan) for 1 min, followed by imaging using a chemiluminescence imaging system (ChemiScope6100; Clinx Science, China). Original images for WB bands are shown in Figure S3.  $\beta$ -Actin was used as the internal control, and the information on the primary and secondary antibodies used is provided in Table 1.

**Table 1** The information on antibody

Name	Dilution rate	Cat number	Source	Company	Country
ETV4	1:1000	AWA45623	Rabbit	Abiowel	China
PKM2	1:2000	AWA43705	Rabbit	Abiowell	China
ALYREF	1:1000	AWA51025	Rabbit	Abiowell	China
PDK1	1:1000	ab202468	Rabbit	Abcam	USA
LDHA	1:1000	19987-1-AP	Rabbit	Proteintech	USA
GLUT1	1:1000	ab115730	Rabbit	Abcam	USA
NSUN2	1:1000	ab259941	Rabbit	Abcam	USA
$\beta$ -actin	1:5000	60008-1-Ig	Mouse	Proteintech	USA
HRP goat anti- mouse IgG (H+L)	1:5000	SA00001-1	/	Proteintech	USA
HRP goat anti- Rabbit IgG (H+L)	1:5000	SA00001-2	/	Proteintech	USA

### Cell counting kit-8 (CCK-8) assay

To evaluate cell viability, the cells were seeded in 24-well plates and allowed to adhere, followed by transfection according to the experimental group for a specified duration. A CCK-8 working solution was prepared by adding CCK-8 reagent (CK04;DOJINDO) to a complete culture medium (the final complete medium contained 10% CCK-8 reagent). Next, the culture medium in the wells was aspirated and replaced with 300  $\mu$ L CCK-8 working solution per well, followed by incubation at 37 °C in an atmosphere of 5% CO<sub>2</sub> for 4 h. Finally, the plate was placed in a multifunctional microplate reader (MB-530; HEALES, China) to measure optical density (OD) at 450 nm.

### Transwell

Approximately, 500  $\mu$ L complete culture medium was added to the lower compartment of a Transwell chamber, while the upper compartment received 100  $\mu$ L HCCC-9810 and RBE cells suspended in serum-free medium. The cells were incubated at 37 °C for 48 h and washed by adding phosphate-buffered saline (PBS) to the upper compartment. Cells were fixed with 4% paraformaldehyde and stained with 0.1% crystal violet. Finally, the cells in the upper compartment were rinsed with water and observed under an inverted microscope (DSZ2000X; Zhongxian Hengye, China).

### Biochemical analysis of GLU, LD, and ATP content

To assess glycolytic metabolism in cells and tumor tissues in mice, the GLU, LD, and ATP assay kits were used to measure the levels of GLU, LD, ATP, malondialdehyde (MDA) and Fe<sup>2+</sup> (A154-1-1; A019-2-1; A095-1-1; A003-1; JL-T1255; Njjcbio, China) in cells, and LD in tumor tissues.

The cell supernatant (2.5  $\mu$ L/well) was added into a 96-well plate containing working solution and standards, mixed well, and incubated at 37 °C for 10 min. Then absorbance value was measured at 505 nm by a multifunctional microplate reader and GLU uptake efficiency was calculated.

The collected cells and tumor tissue samples were broken into homogenate and then centrifuged. The supernatant (0.02 mL/ well) was added to a 96-well plate containing enzyme working solution and color developer, mixed well, and incubated at 37 °C for 10 min. Then the termination solution (2 mL/ well) was added to a 96-well plate and mixed well. The absorbance value was measured at 530 nm and the LD content was calculated.

After centrifugation of the collected cells, the cell precipitate was homogenized and broken in an ice bath. The cell suspension was heated in a boiling water bath, then vortexed and mixed. The mixed sample (30  $\mu$ L/well) was added into a 96-well plate containing substrate solution and promoter, then incubated in a water bath at 37 °C for 30 min. Precipitant (50  $\mu$ L/well) was added into the plate, mixed well, and centrifuged. The supernatant (300  $\mu$ L/well) was taken, and the color development solution was added and mixed well, incubated at room temperature for 2 min, then the terminator was added. The absorbance value was measured at 636 nm and 0.5 cm aperture and the ATP content was calculated.

The cell homogenate, anhydrous ethanol, and MDA reagent were added to the centrifuge tube, vortexed and mixed well, and incubated in a water bath at 95 °C for 40 min. The tube was then cooled with running water and centrifuged. The supernatant was taken to measure absorbance at 532 nm and 1 cm aperture and calculate the MDA content.

The cell homogenate was centrifuged after ultrasonic crushing. The supernatant (120  $\mu$ L) was added into the centrifugal tube containing the assay reagent, mixed well, and placed at room temperature for 15 min. 200  $\mu$ L of the supernatant was taken to measure absorbance at 562 nm, and the Fe<sup>2+</sup> content was calculated.

### Chromatin Immunoprecipitation (ChIP)

To validate whether ETV4 interacts with PKM2 and ALYREF separately, cell pellets were collected. Following the instructions provided by the ChIP assay kit (ab500; Abcam), sequential steps were performed, including cross-linking, sonication, detection of DNA fragment

lengths, immunoprecipitation, de-crosslinking, and DNA purification. Finally, the purified DNA was used for RT-qPCR.

#### Flow cytometry (FCM)

To detect intracellular levels of ROS, two cell types were first collected and incubated with C11-BODIPY (MX5211-1MG; MKBio, China) at 37 °C. After incubation, the cells were washed twice with PBS and the supernatant was discarded after centrifugation. Finally, the cell pellets were resuspended in 300 µL PBS and analyzed using a flow cytometer (A00-1102; Beckman, USA).

#### Real-time quantitative polymerase chain reaction (RT-qPCR)

To evaluate the expression levels of PKM2, ALYREF, and NSUN2 in the cells, total RNA was extracted using TRIzol reagent (15596026; Thermo, USA). The extracted RNA was reverse-transcribed into cDNA using an mRNA reverse transcription kit (CW2569; Cowin Bio), followed by mixing with Ultra SYBR Mixture (CW2601; Cowin Bio).  $\beta$ -Actin was used as the internal reference gene, and relative gene expression was calculated using the  $2^{-\Delta\Delta C_t}$  method. Primer sequences used in the experiments are listed in Table 2.

#### Enzyme-linked immunosorbent assay (ELISA)

The levels of malondialdehyde (MDA) and  $Fe^{2+}$  in the cells were measured using MDA and  $Fe^{2+}$  assay kits (A003-1; JL-T1255; Njcbio) respectively. The OD values of the samples were measured at 532 nm and 562 nm using a multifunctional microplate reader.

#### RNA Immunoprecipitation (RIP)

The cell pellets were mixed with RIPA Lysis Buffer (RIP-12RXN, Sigma, USA) and incubated them. Subsequently, the instructions of the RIP kit (RIP-12RXN; Sigma) and m5C MeRIP Kit (GS-ET-003; cloud-seq, China) were followed for magnetic bead preparation and immunoprecipitation experiments. Total RNA was purified using TRIzol (15596026; Sigma), and cDNA was synthesized using a reverse transcription kit (CW2569; Cowin Bio). Finally, the cDNA was used for RT-qPCR experiments.

**Table 2** Primer sequences

Gene	Sequence	Length
PKM2	F CGTCATTCATCCGCAAGGCAT	159 bp
	R CACGAGCCACCATGATCCCA	
ALYREF	F GGCAGCACGATCTTTTCGAC	186 bp
	R CTGTTCTAAGCTGCGACCA	
NSUN2	F GCTACCCCGAGATCGTCAAG	154 bp
	R TCAGGATACCTTTTGTAAACAGT	
$\beta$ -actin	F ACCCTGAAGTACCCATCGAG	224 bp
	R AGCACAGCCTGGATAGCAAC	

#### RNA stability assay

Approximately, 2 µg/mL Actinomycin D (SBR00013, Sigma-Aldrich, USA) was added to the transfected cells to inhibit mRNA synthesis. Cells were then collected at designated time points according to the grouping, and total RNA was extracted. Finally, the transcript-level expression of PKM2 was determined by RT-qPCR, and the half-life was calculated.

#### Bioinformatic analysis

The expression of ETV4, PKM2, and ALYREF were analyzed in both normal tissues and cholangiocarcinoma using the TCGA database (<https://cancergenome.nih.gov/>), from which the relevant data were downloaded. Subsequently, survival and correlation analyses for ETV4, PKM2, and ALYREF were performed. Concurrently, by utilizing PROMO and JASPAR, ETV4's association with PKM2 and ALYREF was predicted.

#### 5-Ethynyl-2'-deoxyuridine (EdU)

To detect the proliferation of ICC cells, according to the instructions of the EdU detection kit (C10310, RiboBio, China), an EdU medium (50 µM) was first prepared by mixing EdU solution with cell culture medium. Subsequently, the cells were incubated with 100 µL/well of the EdU medium. On the second day, the culture medium was removed, and cells were washed with PBS before adding 4% paraformaldehyde (50 µL/well). Subsequently, glycine (2 mg/mL) was added to the cells and incubated on a shaker for 5 min, after which the solution was removed. Then, the cells were washed with PBS, and the permeabilization solution was added. After washing with PBS, the cells were stained with Apollo and DNA.

#### Terminal Deoxynucleotidyl transferase-mediated dUTP nick-end labeling (TUNEL)

To detect apoptosis, the ICC cells immobilized on slides were sequentially fixed with 4% paraformaldehyde, permeabilized with Triton X-100 (P0096-100 mL; Beyotime), rinsed with PBS, and incubated with 1× Equilibration Buffer (40306ES50; YeasenBio, China). Subsequently, the cells were incubated with the TdT reaction buffer at 37 °C in the dark. This was followed by rinsing with PBS, staining the nuclei with DAPI working solution, rinsing again with PBS, mounting the slides using Fluoromount-G® (0100-01; SouthernBiotech, China), and observing under a microscope.

#### In vivo studies

A total of 24 four-week-old male nude mice (purchased from SJA Laboratory Animal Co., Ltd., Hunan, China) weighing approximately 20 g were acclimatized for one week. Subsequently,  $3 \times 10^6/0.1$  mL HCCC-9810 cells were injected subcutaneously into the left axillary region

of the forelimb of each mouse [25]. Then, the mice bearing tumors were randomly divided into four groups ( $n=6$ ): oe-NC-1+sh-NC group (HCCC-9810 cells transfected with empty vector), oe-ETV4+sh-NC group (HCCC-9810 cells transfected with oe-ETV4+sh-NC), oe-NC+sh-ALYREF group (HCCC-9810 cells transfected with oe-NC+sh-ALYREF), and oe-ETV4+sh-ALYREF group (HCCC-9810 cells transfected with oe-ETV4+sh-ALYREF). After injection, tumor size was measured every 7 d. Tumor volume was calculated using the following formula:  $(\text{length axis} \times \text{width axis}^2)/2$ . On the 28th d, mice were euthanized by cervical dislocation following the administration of sodium pentobarbital. The subcutaneous xenografts were photographed and collected.

### Statistical analysis

Data were analyzed using GraphPad Prism9.0. Data are presented as mean  $\pm$  standard deviation (SD). After checking for homogeneity of variance and normality, the data were compared. Comparisons between two groups were performed using unpaired *t*-tests, whereas comparisons among multiple groups were performed using a one-way ANOVA and Tukey's post-hoc test. Two-way ANOVA was used to evaluate the differences between different time points and among multiple groups.  $P < 0.05$  indicates significance.

## Results

### ETV4 and PKM2 enhance ICC cell proliferation and glycolytic metabolism

To explore the impact of ETV4 and PKM2 on ICC, we initially analyzed their expression in ICC samples. The results showed that both ETV4 and PKM2 were highly expressed in ICC, and high expression of ETV4 and PKM2 resulted in shorter survival (compared to what is observed when their expression is low) (Fig. 1A-B). For overexpression experiments, HCCC-9810 and RBE were transfected with overexpression plasmids for ETV4 and PKM2. NC-1 and NC-2 were control plasmids for the overexpression of ETV4 and PKM2, respectively, and the overexpression efficiency of ETV4 and PKM2 was 232% and 258%, and 852% and 403% in RBE cells. The expression of PKM2 increased with elevated expression of ETV4, and no significant change in the expression of ETV4 was observed when the expression of PKM2 was elevated (Fig. 1C). Furthermore, ETV4 and PKM2 were observed to enhance cell proliferation and migration (Fig. 1D-F), improve GLU utilization, LD production, and intracellular ATP generation (Fig. 1G-I), and promote the expression of glycolysis-related proteins (PDK1, LDHA, and GLUT1) (Fig. 1J). The results of PROMO and JASPAR predictions indicated that ETV4 may interact with two sites on PKM2, and CHIP experiments confirmed

that ETV4 binds to the PKM2 promoter (Fig. 1K-L). Additionally, studies have reported the presence of PKM2 in tetrameric and dimeric forms [9]. Our results showed that the content of dimeric form of PKM2 increased after transfection of oe-ETV4 plasmid, while the content of dimeric form of PKM2 decreased after transfection of sh-ETV4 plasmid. There was no significant change in the content of the tetrameric form in the above four groups (Figure. S1A). These results suggest that ETV4 stimulates PKM2 expression and that both ETV4 and PKM2 promote ICC cell proliferation and glycolytic metabolism.

### ETV4 promotes the resistance of ICC cells to ferroptosis through PKM2-mediated glycolytic metabolism

To investigate whether ETV4 affects the proliferation and glycolytic metabolism of ICC cells by regulating PKM2, we first transfected cells with ETV4-interfering and PKM2-overexpressing plasmids. The knockdown efficiency of ETV4 in the protein bands was 73% and 88% in HCC-9810 and RBE cells, separately. A significant decrease in the expression of ETV4 and PKM2 was observed after sh-ETV4 treatment. Conversely, after oe-PKM2 treatment, PKM2 expression was elevated, while the ETV4 expression remained unaffected (Fig. 2A). In sh-ETV4 cells, the proliferation, migration, GLU utilization, LD production, and intracellular ATP generation were decreased; these results were contradictory to those observed in case of oe-PKM2. Cell proliferation, migration, and glycolysis in the oe-PKM2+sh-ETV4 group were significantly higher than those in the oe-NC-1+sh-ETV4 group, indicating that oe-PKM2 reversed the inhibition effect of sh-ETV4 (Fig. 2B-G). Additionally, oe-PKM2 reversed the inhibition effect of sh-ETV4 on the expression of glycolysis-related proteins (Fig. 2H). TUNEL assay showed that ETV4 knockdown led to an increase in apoptosis rate. In addition, oe-PKM2 reversed the effect of sh-ETV4 (Figure S2A). These results indicated that ETV4 regulates the glycolytic metabolism in ICC cells by modulating the expression of PKM2. Studies have demonstrated that LD present in the extracellular environment, resulting from cellular glycolytic metabolism, can contribute to the resistance against ferroptosis in cancer cells [26]. In previous experiments, we demonstrated that ETV4 positively regulates the expression of PKM2. Therefore, we speculated that ETV4 mediates the development of resistance against ferroptosis in ICC cells via PKM2. To further probe the effects of ETV4 and PKM2 on ICC cell ferroptosis, we treated HCCC-9810 and RBE cells with the ferroptosis inducer Erastin. An optimal concentration of Erastin, which caused half-maximal cell death, was then used in later experiments (Fig. 2I). The experimental results showed that compared with oe-NC-1+sh-NC+Erastin, the oe-PKM2+sh-NC+Erastin group promoted the

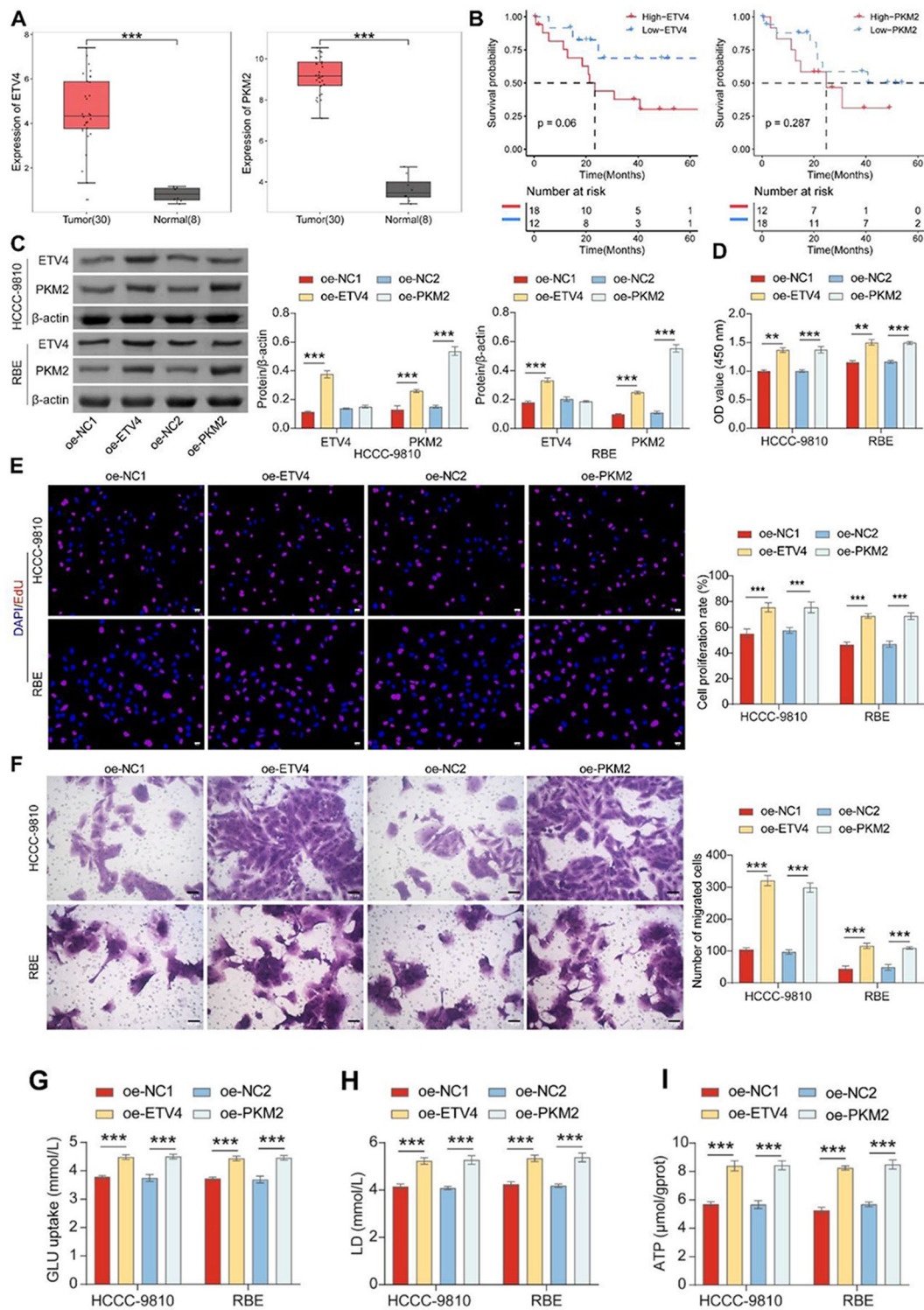


**Fig. 1** ETV4 and PKM2 enhance ICC cell proliferation and glycolytic metabolism. **(A)** High expression levels of ETV4 and PKM2 in ICC were analyzed using the TCGA database. **(B)** The analysis of the survival rate in the presence of ETV4 and PKM2. **(C)** The expression levels of ETV4 and PKM2 were detected by WB. **(D)** Cell proliferation was measured by CCK-8 assay. **(E)** ICC cell proliferation was detected by the EdU assay (Magnification:  $\times 50$ , scale bar = 200  $\mu\text{m}$ ). **(F)** Cell migration of ICC cells was assessed by Transwell assay (Magnification:  $\times 100$ , scale bar = 100  $\mu\text{m}$ ). **(G-I)** Measurement of the GLU, LD, and ATP content in ICC cells. **(J)** Expression of PDK1, LDHA, and GLUT1 was assessed by WB. **(K)** Bioinformatics prediction of binding sites between ETV4 and PKM2. **(L)** ChIP validation of the binding of ETV4 and the promoter of ALYREF. \* $P < 0.05$ ; \*\* $P < 0.01$ ; \*\*\* $P < 0.001$ ;  $n = 3$

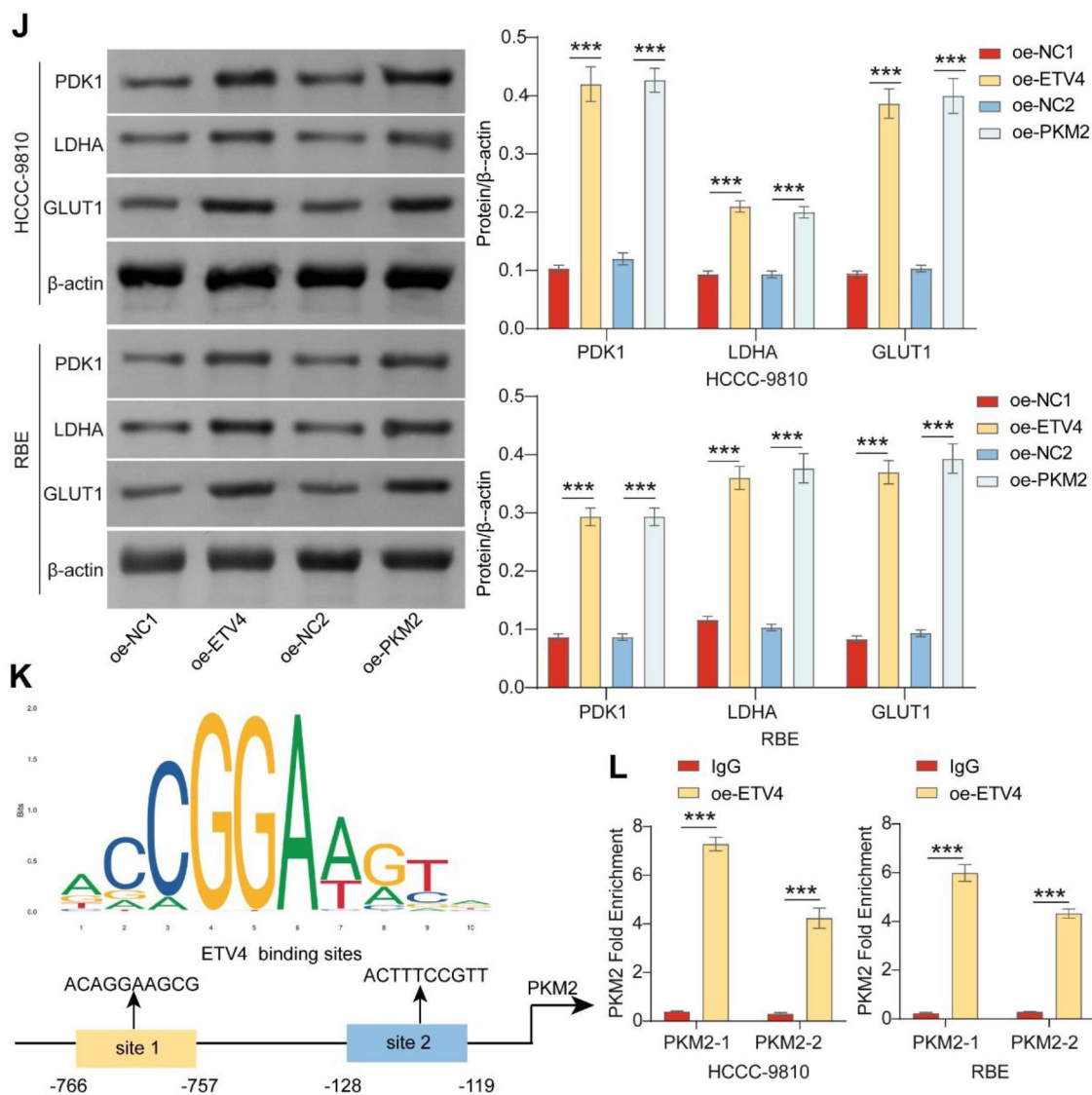


**Fig. 1** (continued)

proliferation and migration of ICC cells (Fig. 2J-K), while simultaneously reducing lipid ROS, MDA, and  $Fe^{2+}$  levels (Fig. 2L-M), and the oe-NC-1 + sh-ETV4 + Erastin group showed the opposite results. sh-ETV4 could attenuate the cellular resistance to ferroptosis, while oe-PKM2 could reverse this effect. Notably, ETV4 may boost glycolytic metabolism by regulating PKM2 expression, subsequently facilitating resistance to ferroptosis in ICC cells.

#### ALYREF contributes to the resistance of ICC cells to ferroptosis through PKM2-mediated glycolytic metabolism

To investigate the potential role of ALYREF in modulating PKM2 expression and its effect on ICC cells, the expression of ALYREF in ICC was analyzed. Notably, ALYREF was highly expressed in ICC, and patients with high ALYREF expression had a reduced survival

period and probability (Fig. 3A-B). Subsequently, the ALYREF knockdown plasmid was transfected into two types of ICC cells, which led to a significant reduction in ALYREF expression, indicating successful knockdown of ALYREF. The knockdown efficiency of ALYREF was 74% and 80% in HCC-9810 and RBE cells, separately. With reduced ALYREF expression, the expression levels of PKM2 decreased (Fig. 3C-D), and dimeric PKM2 decreased with no significant change in the tetrameric form (Figure S1B). Subsequent experiments showed that with reduced ALYREF expression, the levels of cell proliferation, migration, GLU utilization, LD production, and intracellular ATP generation decreased, which was contrary to the results obtained upon PKM2 overexpression. oe-PKM2 reversed the promoting effect of sh-ALYREF (Fig. 3E-J). Additionally, the expression

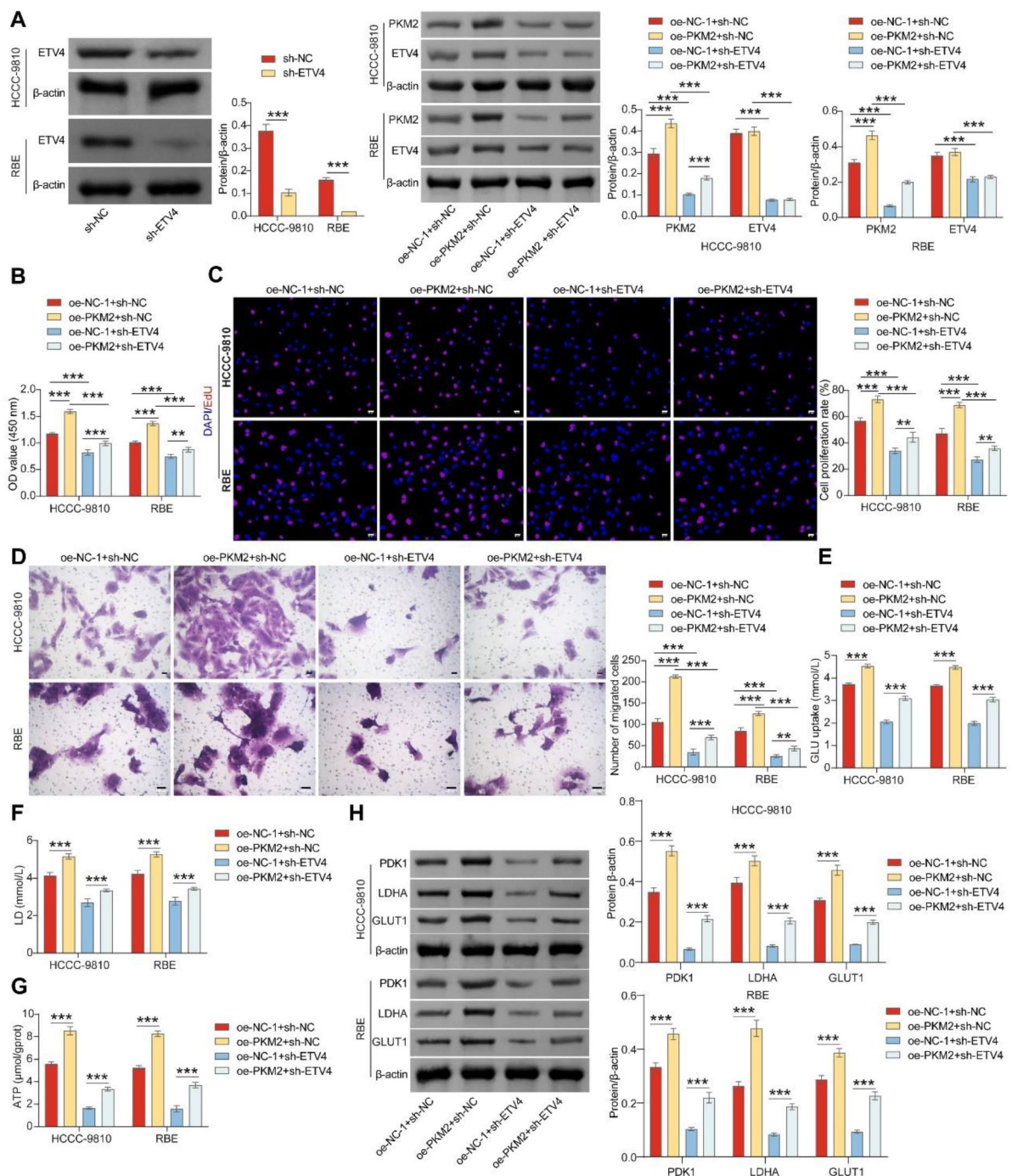


**Fig. 2** ETV4 promotes ICC cell resistance to ferroptosis through PKM2-mediated glycolytic metabolism. **(A)** The expression levels of ETV4 and PKM2 were detected by WB. **(B)** ICC cell proliferation was assessed by CCK-8 assay. **(C)** ICC cell proliferation was detected by the EdU assay (Magnification:  $\times 50$ , scale bar = 200  $\mu$ m). **(D)** ICC cell migration was examined by Transwell assay (Magnification:  $\times 100$ , scale bar = 100  $\mu$ m). **(E-G)** Measurement of GLU, LD, and ATP content in ICC cells. **(H)** The expression of PDK1, LDHA, and GLUT1 assessed by WB. **(I)** CCK-8 assay was used to screen Erastin concentration. **(J)** ICC cell proliferation was assessed by CCK-8 assay. **(K)** Transwell assay was used to evaluate ICC cell migration after erastin induction (Magnification:  $\times 100$ , scale bar = 100  $\mu$ m). **(L)** FCM was used to measure ICC cell lipid ROS levels. **(M)** ELISA was used to detect MDA and  $Fe^{2+}$  levels in ICC cells. \* $P < 0.05$ ; \*\* $P < 0.01$ ; \*\*\* $P < 0.001$ ;  $n = 3$

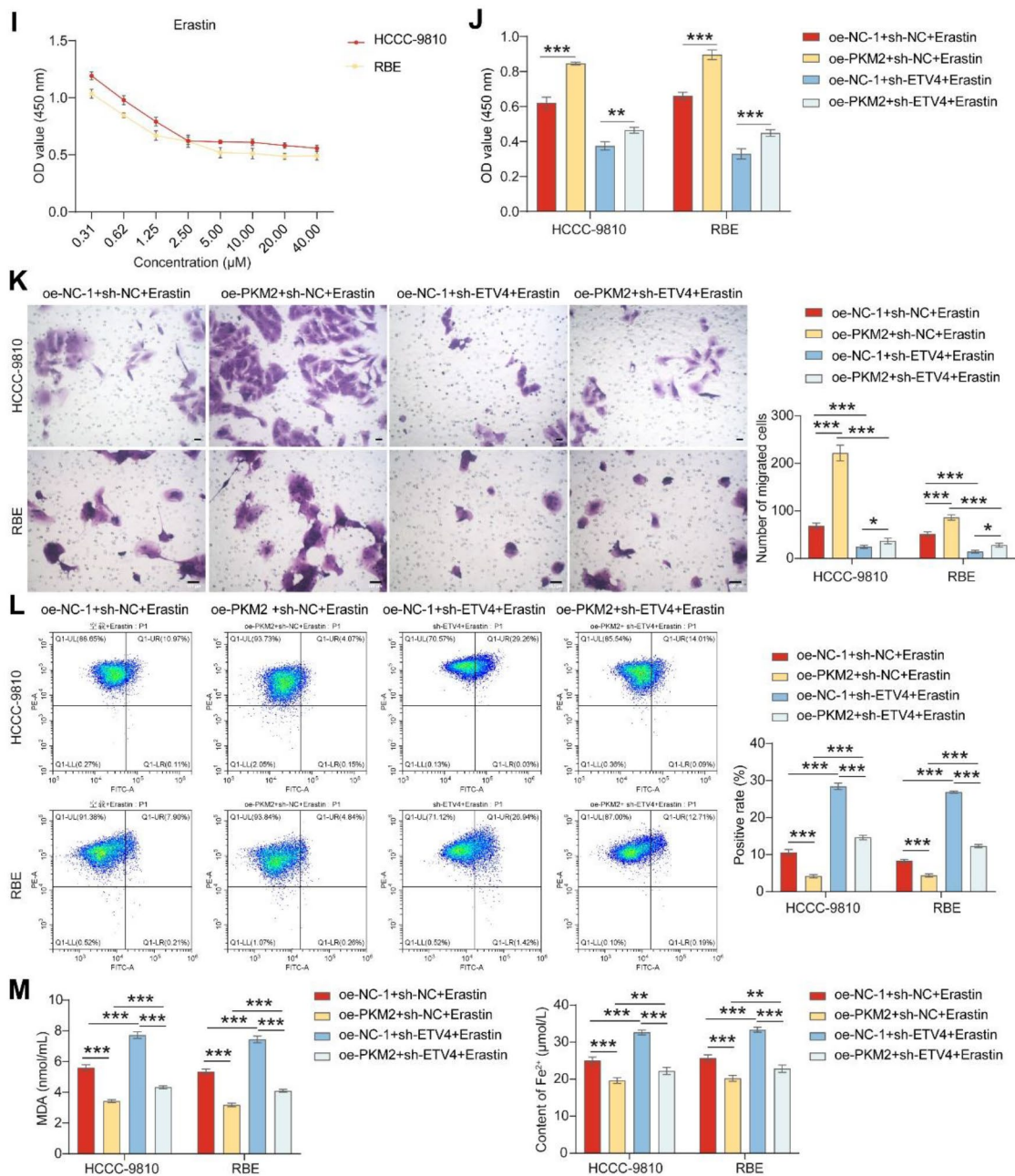


Fig. 2 (continued)

of glycolysis-related proteins decreased with a reduction in ALYREF expression (Fig. 3K). ALYREF knock-down increased the rate of apoptosis, and oe-PKM2 reversed the effect of sh-ALYREF (Figure S2B). Following the induction of ferroptosis with Erastin, the results showed that compared with oe-NC-1 + sh-NC + Erastin, sh-ALYREF + oe-NC-2 + Erastin decreased cell proliferation and migration, while simultaneously promoting lipid ROS, MDA, and  $\text{Fe}^{2+}$  levels, which was contrary to the results obtained with oe-PKM2. Moreover, oe-PKM2 reversed the promotional effects of sh-ALYREF

on ferroptosis resistance (Fig. 3L-P). These findings suggest that ALYREF promotes the expression of PKM2 and contributes to the resistance of ICC cells to ferroptosis through PKM2-mediated glycolytic metabolism.

#### ALYREF stabilizes PKM2 mRNA through an m5C-dependent mechanism

m5C, a post-transcriptional RNA modification, is regulated by various factors, including the “reader” protein ALYREF [27]. The study reported that ALYREF stabilizes PKM2 mRNA in bladder cancer [11]. We

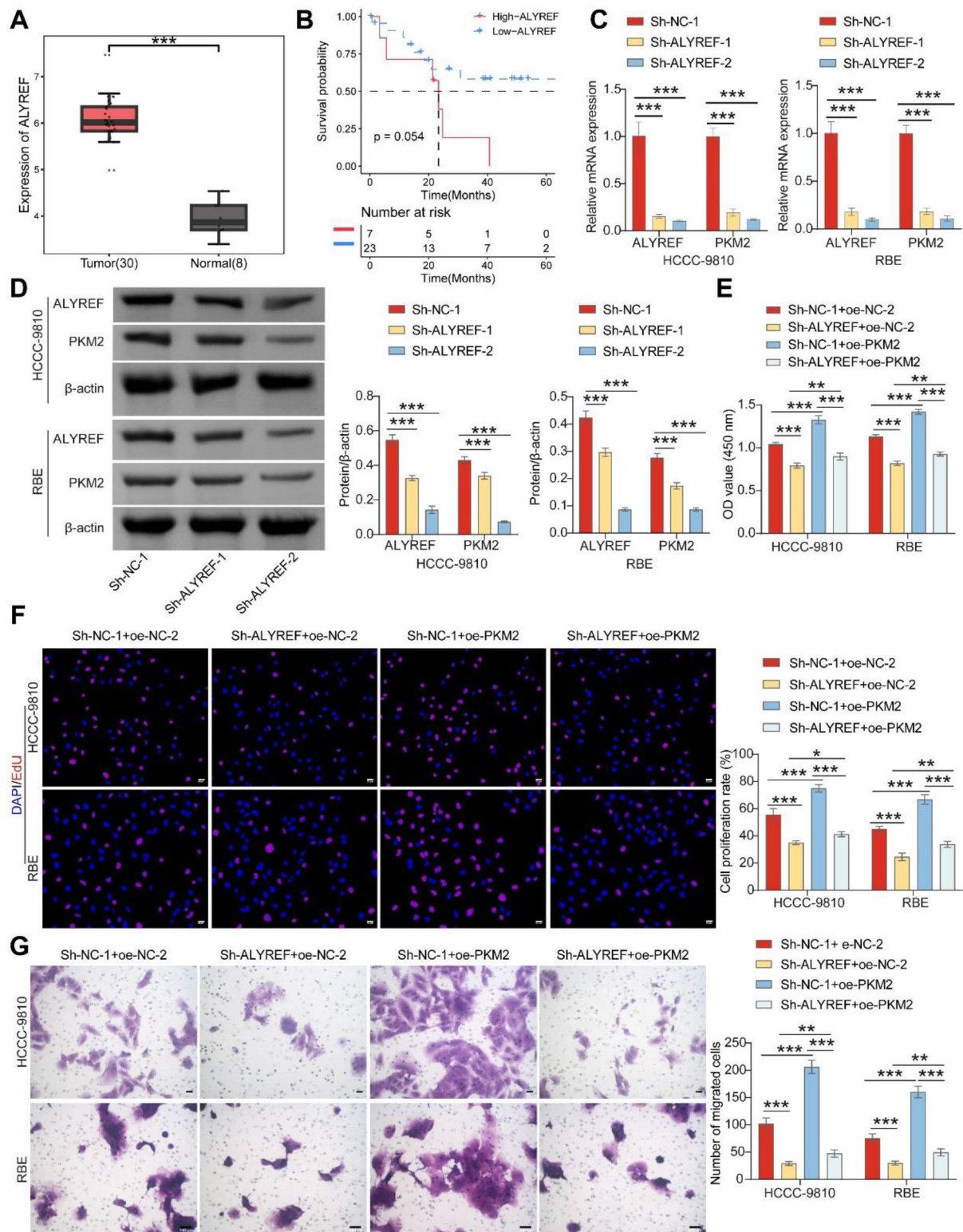


**Fig. 3** ALYREF contributes to ICC cell resistance to ferroptosis through PKM2-mediated glycolytic metabolism. **(A)** High expression level of ALYREF in ICC was analyzed using the TCGA database. **(B)** The analysis of the survival rate in the presence of ALYREF and PKM2. **(C–D)** The expression levels of ALYREF and PKM2 were analyzed by RT-qPCR and WB. **(E)** ICC cell proliferation was assessed by CCK-8 assay. **(F)** ICC cell proliferation detected by Edu assay (Magnification:  $\times 50$ , scale bar = 200  $\mu$ m). **(G)** ICC cell migration was examined by Transwell assay (Magnification:  $\times 100$ , scale bar = 100  $\mu$ m). **(H–J)** Measurement of GLU, LD, and ATP content in ICC cells. **(K)** The expression levels of PDK1, LDHA, and GLUT1 assessed by WB. **(L)** ICC cell proliferation was assessed by CCK-8 assay. **(M)** Transwell assay was used to evaluate ICC cell migration after Erastin induction (Magnification:  $\times 100$ , scale bar = 100  $\mu$ m). **(N)** FCM was used to measure ICC cell lipid ROS levels. **(O)** ELISA was used to detect MDA and  $Fe^{2+}$  levels in ICC cells. \* $P < 0.05$  vs. sh-NC-1; \*\* $P < 0.01$ ; \*\*\* $P < 0.001$ ;  $n = 3$

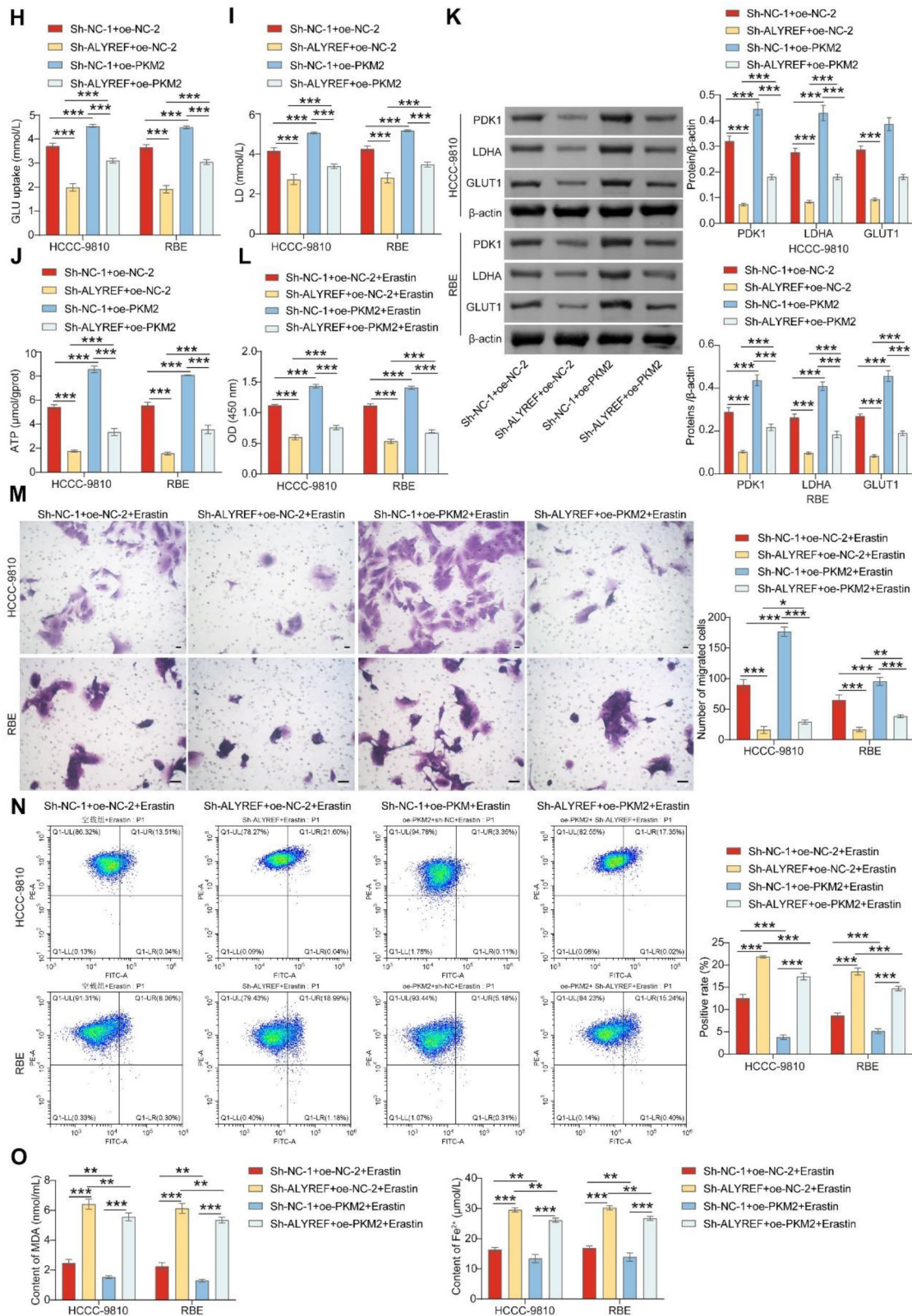


**Fig. 3** (continued)

hypothesized that ALYREF could bind to PKM2 mRNA, and first verified the binding between ALYREF and

PKM2 (Fig. 4A). Concurrently, the expression levels of PKM2 decreased with a reduction in ALYREF (Fig. 4B-C). After treating the cells with actinomycin D, the stability of PKM2 mRNA was evaluated. The degradation of PKM2 mRNA accelerated following the down-regulation of ALYREF (Fig. 4D). The formation of m5C in mRNA is primarily catalyzed by the RNA methyltransferase NSUN2 [27, 28]. ETV4 stabilizes PKM2 expression upon binding to the NSUN2 promoter [29]. Therefore, we selected NSUN2 as the m5C-dependent mechanism. We transfected the cells with NSUN2 interference plasmids, which led to a reduced expression of NSUN2. The knockdown efficiency of NSUN2 was 72% and 78% in HCC-9810 and RBE cells, separately (Fig. 4E-F). Using m5C-RIP to detect the enrichment of PKM2, the m5C writer NSUN2 knockdown resulted in a decrease in the enrichment of PKM2 (Fig. 4G). Based on these data, we deduce that ALYREF stabilizes PKM2 mRNA via an m5C-dependent pathway.

### ETV4 targets and regulates ALYREF to promote ICC cell proliferation

To investigate whether ETV4 targets and regulates ALYREF, we first discovered a positive correlation between ETV4 and ALYREF (Fig. 5A). When the expression of ALYREF was reduced, the promoting effects of ETV4 on PKM2 expression levels as well as on cell proliferation and migration in ICC were attenuated (Fig. 5B-E). Furthermore, the results of PROMO and JASPAR predictions indicated two binding sites may be between ETV4 and ALYREF. We further validated that ETV4 can bind to the ALYREF promoter using a ChIP assay (Fig. 5F-G). Based on these data, ETV4 could be said to target and regulate ALYREF, thereby promoting ICC cell proliferation.

### The ETV4/ALYREF axis promotes tumor proliferation and glycolytic metabolism in mice

To investigate the effects of ETV4 and ALYREF on ICC, we conducted *in vivo* experiments using mice. After transfection with *oe*-ETV4, the volume and weight of the tumors in mice increased. However, when transfected

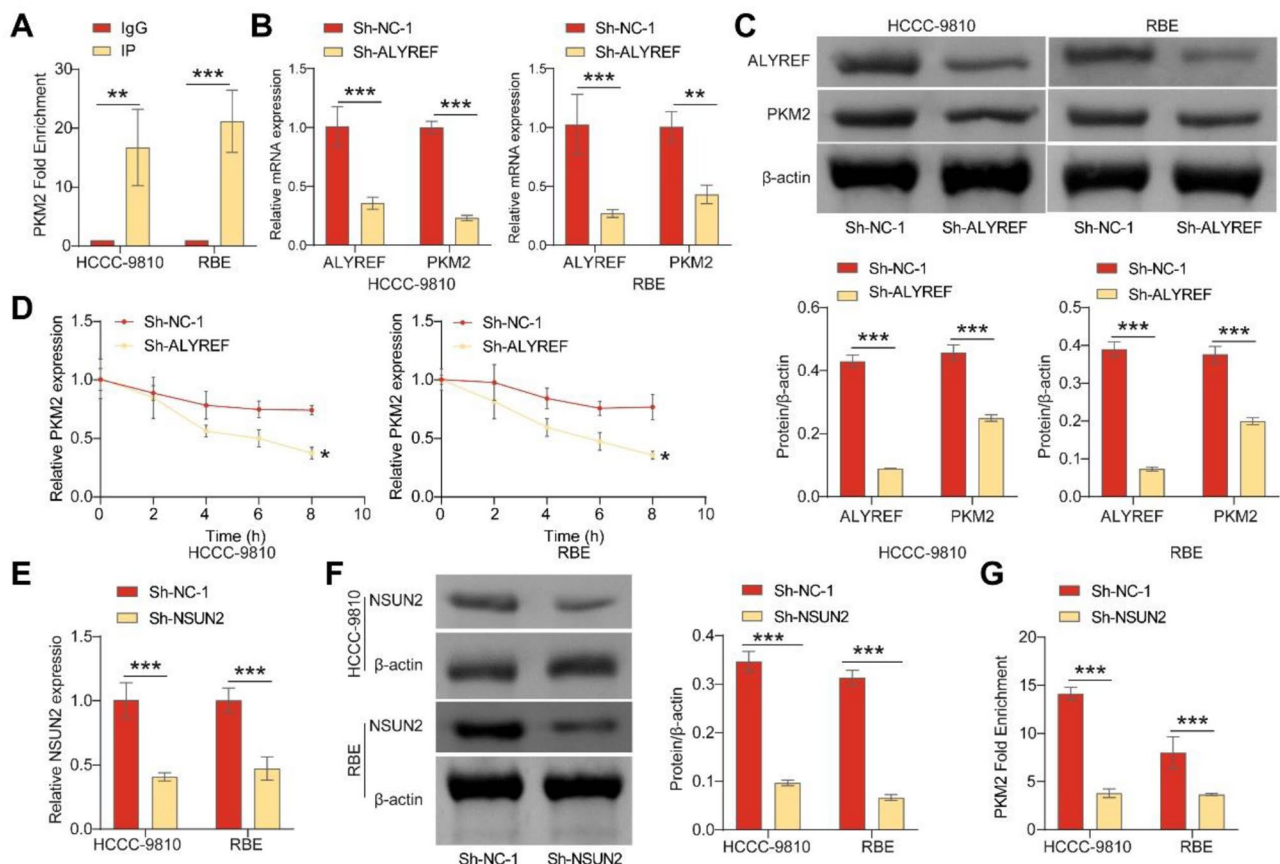


**Fig. 4** ALYREF stabilizes PKM2 mRNA through an m5C-dependent mechanism. **(A)** RIP assay revealed the binding between ALYREF and PKM2 in ICC cells. **(B)** The expression of ALYREF and PKM2 in ICC cells detected by RT-qPCR. **(C)** The expression of ALYREF and PKM2 in ICC cells detected by WB. **(D)** Following treatment with Actinomycin D, the degradation condition of PKM2 mRNA was detected. **(E)** The expression of NSUN2 in ICC cells analyzed by RT-qPCR. **(F)** The expression of NSUN2 in ICC cells examined by WB. **(G)** The enrichment level of PKM2 detected using m5C-RIP. \* $P < 0.05$ ; \*\* $P < 0.01$ ; \*\*\* $P < 0.001$ ;  $n = 3$

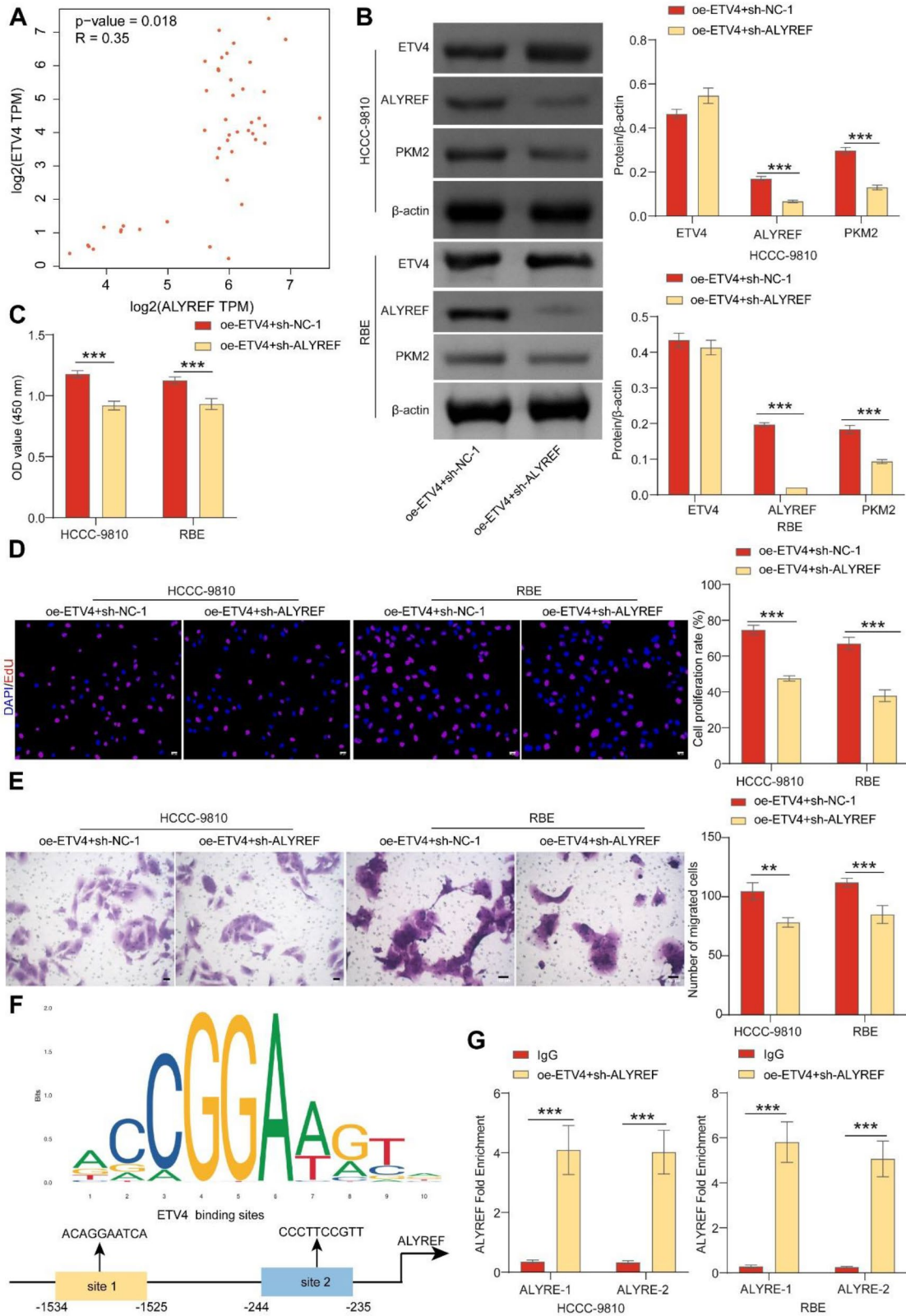


**Fig. 5** (See legend on next page.)

(See figure on previous page.)

**Fig. 5** ETV4 targets and regulates ALYREF to promote ICC cell proliferation. **(A)** ETV4 was positively correlated with ALYREF. **(B)** The expression of ETV4, ALYREF, and PKM2 in ICC cells detected by WB. **(C)** ICC cell proliferation assessed by CCK-8 assay. **(D)** ICC cell proliferation detected by EdU assay (Magnification:  $\times 50$ , scale bar = 200  $\mu\text{m}$ ). **(E)** ICC cell migration examined by Transwell assay (Magnification:  $\times 100$ , scale bar = 100  $\mu\text{m}$ ). **(F)** Bioinformatic prediction of binding sites between ETV4 and ALYREF, and ALYREF's motif diagram. **(G)** ChIP validation of the binding of ETV4 and ALYREF to the promoter. \* $P < 0.05$ ; \*\* $P < 0.01$ ; \*\*\* $P < 0.001$ ;  $n = 3$

with si-ALYREF, tumor volume and weight decreased. Moreover, si-ALYREF reversed the effect of oe-ETV4, resulting in decreased tumor volume and weight (Fig. 6A-C). Following transfection with oe-ETV4, the levels of LD in the tumor cells of the mice increased. Conversely, transfection with si-ALYREF led to a decrease in LD levels in tumor cells, and si-ALYREF reversed the effect of oe-ETV4, causing a decrease in LD levels (Fig. 6D). Furthermore, after transfection with oe-ETV4, the expression of proteins downstream of PKM2 increased, whereas transfection with si-ALYREF decreased the expression of these proteins. This effect of si-ALYREF was reversed by oe-ETV4 treatment (Fig. 6E). Based on these data, we concluded that ETV4/ALYREF could regulate the expression of PKM2 and promote ICC proliferation and glycolytic metabolism.

## Discussion

ICC is a malignant tumor with a high fatality rate, making it a focal point of clinical research [30]. However, studies on the pathogenesis of ICC are scarce. Therefore, to improve the survival rate of patients with ICC, we aimed to identify new molecular targets for treatment. *ETV4* is a gene associated with ferroptosis [31]. *ETV4* has been studied in cancer research, and its overexpression has been observed in various cancers such as esophageal and gastric cancers; however, reports of its involvement in ICC are rare [32–34]. In the present study, we explored the effects of *ETV4* on ICC to elucidate its potential mechanisms of action.

PKM2 is one of the important targets in cancer, which can regulate glycolytic metabolism [35]. Yu et al. found that PKM2 is highly expressed in ICC, and knockdown of PKM2 can inhibit the value-added of ICC cells [36]. Ubiquitin-specific protease 28 (USP28) can promote glycolysis through mediating PKM2, which in turn promotes the progression of Cholangiocarcinoma [37]. DDX39B can promote glycolysis in colon cancer cells and enhance the stabilization of PKM2 [38]. Ding et al. found that ETV4/NSUN2 regulated the expression of PKM2 [39]. ETV4 promotes the growth of cholangiocarcinoma [23, 40] and also promotes glycolysis in breast cancer cells [41]. Our results showed that ETV4 and PKM2 were highly expressed in ICC, overall survival (OS) in ICC patients decreased with elevated expression of ETV4 and PKM2, and ETV4 and PKM2 promoted the proliferation, migration, and glycolytic metabolism of ICC cells. PKM2 plays a role in promoting aerobic glycolysis and

can switch between a highly active tetrameric form and a less active dimeric form in healthy tissues but generally exists in a dimeric form in tumor cells [42]. Dimeric PKM2 translocates to the nucleus and acts as a co-activator of transcription factors [43]. Additionally, Oridonin can reduce the expression of PKM2 dimer in cancer to reverse the Warburg effect, ultimately inhibiting the development of colorectal cancer [44]. Therefore the level of dimerization expression of PKM2 is important in cancer growth. Our results showed that ETV4 could bind to the promoter of PKM2, and PKM2 dimer was elevated after the elevation of ETV4 expression, while PKM2 tetramer did not change significantly. Knockdown of ETV4 reversed the promotion of PKM2 on glycolytic metabolism. The above results suggested that ETV4 promotes glycolytic metabolism and ICC cell proliferation by promoting PKM2 dimer expression.

Ferroptosis plays an important role in tumor development, and elevated levels of ferroptosis can inhibit the proliferation of ICC cells [45]. Ferroptosis is usually accompanied by iron accumulation and lipid peroxidation, with MDA being a product of lipid peroxidation [46]. The reduction of ETV4 encourages ferroptosis by inhibiting the production of SLC7A11 [47]. Melatonin can inhibit ferroptosis by activating PKM2 [48]. Furthermore, in hepatocellular carcinoma, PD-L1 mitochondrial translocation enhances glycolytic metabolism, which mediates GPX4-dependent resistance to ferroptosis [49]. Elevated lactate levels in the extracellular environment of hepatocellular carcinoma cells promote ferroptosis resistance in cancer cells due to the onset of glycolysis [26]. Our results showed that ETV4 and PKM2 promote ferroptosis resistance in ICC cells, and knockdown of ETV4 reversed the promotion of ferroptosis resistance by PKM2.

Previous studies have shown that ALYREF promotes neuroblastoma growth and ETV4 promotes hepatocellular carcinoma growth, which aligns with our findings [50, 51]. Aberrant PKM2 expression can promote the occurrence of malignant tumors, and the expression of PKM2 is regulated by ALYREF [11, 52]. We found that ETV4 and ALYREF were able to bind, ALYREF expression was reduced, PKM2 monomer and PKM2 dimer were reduced, tetrameric forms were not significantly changed, and knockdown of ALYREF reversed the promotion of PKM2 on glycolytic metabolism and ferroptosis resistance. Therefore, we could conclude that ETV4 and ALYREF may promote glycolytic metabolism by

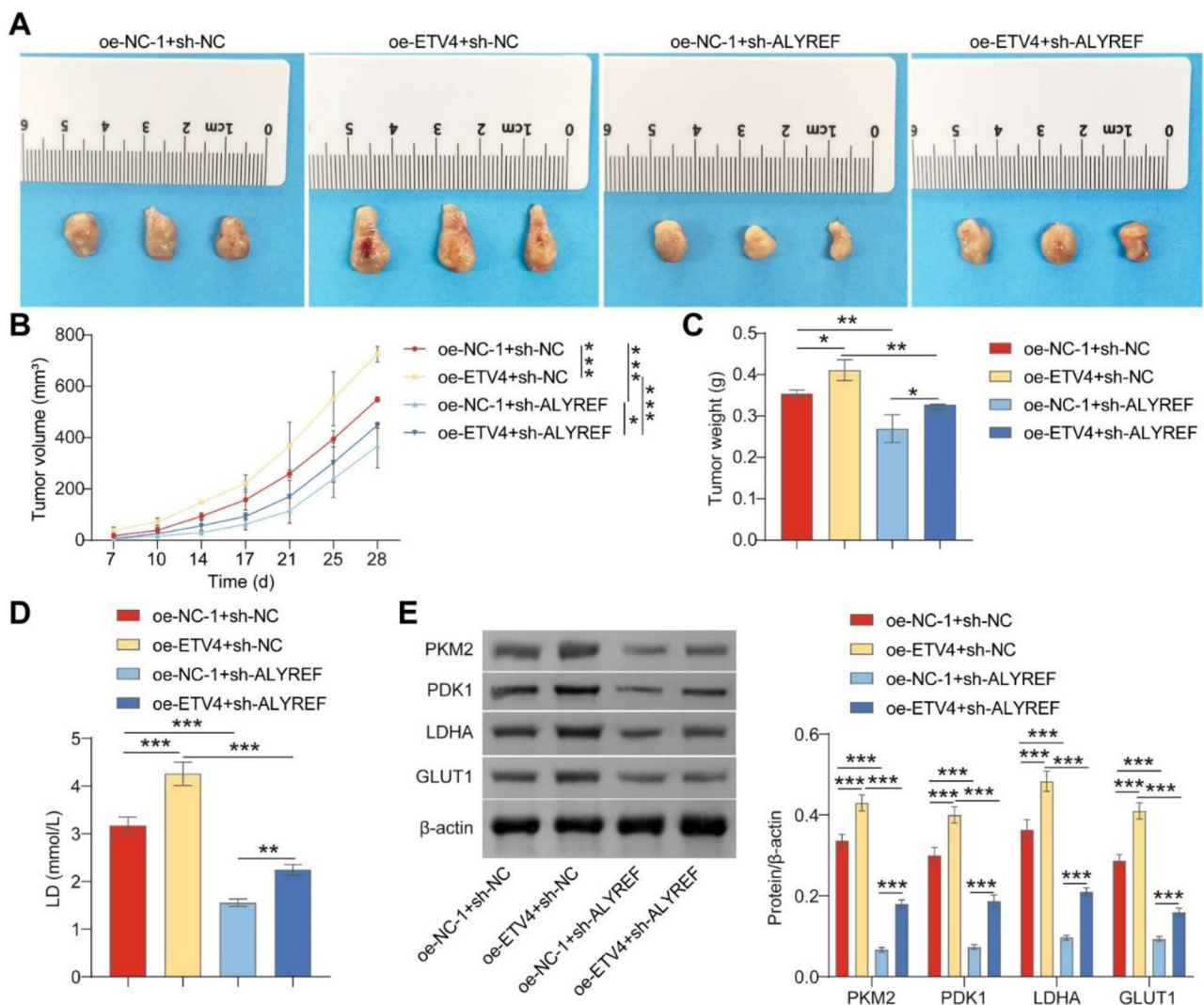


**Fig. 6** The ETV4/ALYREF axis promotes tumor proliferation and glycolytic metabolism in mice. **(A)** Images of subcutaneous xenograft in mice. **(B)** The effect of ETV4/ALYREF axis on subcutaneous xenograft volume. **(C)** The effect of ETV4/ALYREF axis on subcutaneous xenografts weight. **(D)** The effect of ETV4/ALYREF axis on the concentration of LD in subcutaneous xenografts. **(E)** WB analysis of the expression of PKM2 and its downstream targets in subcutaneous xenografts. \* $P < 0.05$ ; \*\* $P < 0.01$ ; \*\*\* $P < 0.001$ ;  $n = 6$

facilitating PKM2, leading to elevated lactate levels in the cells, which in turn enhances ferroptosis resistance in ICC cells.

m5C is a post-transcriptional RNA modification that regulates various biological processes, including mRNA stability [27, 28]. m5C is also regulated by various factors, including the “reader” protein ALYREF [27]. The formation of m5C in mRNA is primarily catalyzed by the RNA methyltransferase, NSUN2 [27, 28]. Our study confirmed that there is an interaction between ALYREF and PKM2 and that the half-life of PKM2 mRNA is shortened when ALYREF expression is reduced. Additionally, when the expression of NSUN2 is reduced, PKM2 mRNA enrichment decreases. Therefore, we could conclude that ALYREF stabilizes PKM2 mRNA through an

m5C-dependent mechanism, which is consistent with the findings of Jingzi et al. [11]. However, there are some limitations to our study, as we only validated our results through in vitro cell culture experiments and mouse models. Additionally, we have not yet investigated specific strategies to address glycolytic dysregulation, which we plan to study in future experiments.

## Conclusion

In our research, we found that *ETV4*, *ALYREF*, and *PKM2* were highly expressed, and *ETV4* and *ALYREF* facilitated the progression of ICC by enhancing ferroptosis resistance through PKM2-mediated glycolytic metabolism. Our results highlighted the potential of *ETV4*, *ALYREF*, and *PKM2* as biomarkers and therapeutic targets for

ICC, unveiling for the first time the regulatory interplay among these genes. Furthermore, these findings offer a novel approach and theoretical foundation for ICC treatment by specifically targeting ferroptosis resistance and glycolytic metabolic pathways.

### Supplementary Information

The online version contains supplementary material available at <https://doi.org/10.1186/s40170-025-00387-1>.

Supplementary Material 1

### Acknowledgements

None.

### Author contributions

Xiaohui Wang: resources, investigation, data curation, validation, Formal analysis, visualization, Writing - original draft and Writing - review & editing. Wenbin Duan, Zhongzhi Ma, Haoquan Wen, Xianhai Mao: data curation. Changjun Liu: conceptualization, methodology, project management, Funding acquisition.

### Funding

This work was supported by Hunan Provincial Natural Science Foundation of China (2023JJ40382).

### Data availability

The data generated during and/or analysed during the current study are not publicly available, and will be made available from the corresponding author on request.

### Declarations

#### Ethics approval and consent to participate

All animal experiments were carried out according to ARRIVE guidelines and approved by the Animal Ethics Committee of Hunan Provincial People's Hospital (approve number: 2024052). No clinical experiment was performed in this study.

#### Consent for publication

Not applicable.

#### Competing interests

The authors declare no competing interests.

Received: 12 October 2024 / Accepted: 7 April 2025

Published online: 22 April 2025

### References

- Pant K, Richard S, Peixoto E, Grailone SA. Role of glucose metabolism reprogramming in the pathogenesis of cholangiocarcinoma. *Front Med (Lausanne)*. 2020;7:113.
- Bridgewater J, Galle PR, Khan SA, Llovet JM, Park JW, Patel T, et al. Guidelines for the diagnosis and management of intrahepatic cholangiocarcinoma. *J Hepatol*. 2014;60(6):1268–89.
- Du J, Lan T, Liao H, Feng X, Chen X, Liao W, et al. CircNFIB inhibits tumor growth and metastasis through suppressing MEK1/ERK signaling in intrahepatic cholangiocarcinoma. *Mol Cancer*. 2022;21(1):18.
- Rizvi S, Gores GJ. Pathogenesis, diagnosis, and management of cholangiocarcinoma. *Gastroenterology*. 2013;145(6):1215–29.
- Zhang H, Yang T, Wu M, Shen F. Intrahepatic cholangiocarcinoma: epidemiology, risk factors, diagnosis and surgical management. *Cancer Lett*. 2016;379(2):198–205.
- Kelley RK, Bridgewater J, Gores GJ, Zhu AX. Systemic therapies for intrahepatic cholangiocarcinoma. *J Hepatol*. 2020;72(2):353–63.
- Wang Y, Li J, Xia Y, Gong R, Wang K, Yan Z, et al. Prognostic nomogram for intrahepatic cholangiocarcinoma after partial hepatectomy. *J Clin Oncol*. 2013;31(9):1188–95.
- Paul S, Ghosh S, Kumar S. Tumor glycolysis, an essential sweet tooth of tumor cells. *Semin Cancer Biol*. 2022;86(Pt 3):1216–30.
- Zhang Z, Deng X, Liu Y, Liu Y, Sun L, Chen F. PKM2, function and expression and regulation. *Cell Biosci*. 2019;9:52.
- Qian Z, Hu W, Lv Z, Liu H, Chen D, Wang Y, et al. PKM2 upregulation promotes malignancy and indicates poor prognosis for intrahepatic cholangiocarcinoma. *Clin Res Hepatol Gastroenterol*. 2020;44(2):162–73.
- Wang JZ, Zhu W, Han J, Yang X, Zhou R, Lu HC, et al. The role of the HIF-1 $\alpha$ /ALYREF/PKM2 axis in Glycolysis and tumorigenesis of bladder cancer. *Cancer Commun (Lond)*. 2021;41(7):560–75.
- Xue C, Gu X, Zheng Q, Shi Q, Yuan X, Su Y, et al. ALYREF mediates RNA m(5)C modification to promote hepatocellular carcinoma progression. *Signal Transduct Target Ther*. 2023;8(1):130.
- Xue C, Zhao Y, Li G, Li L. Multi-Omic analyses of the m(5)C regulator ALYREF reveal its essential roles in hepatocellular carcinoma. *Front Oncol*. 2021;11:633415.
- Zeng C, Lin J, Zhang K, Ou H, Shen K, Liu Q, et al. SHARPIN promotes cell proliferation of cholangiocarcinoma and inhibits ferroptosis via p53/SLC7A11/GPX4 signaling. *Cancer Sci*. 2022;113(11):3766–75.
- Chen X, Kang R, Kroemer G, Tang D. Broadening horizons: the role of ferroptosis in cancer. *Nat Rev Clin Oncol*. 2021;18(5):280–96.
- Xu T, Ding W, Ji X, Ao X, Liu Y, Yu W, Wang J. Molecular mechanisms of ferroptosis and its role in cancer therapy. *J Cell Mol Med*. 2019;23(8):4900–12.
- Manz DH, Blanchette NL, Paul BT, Torti FM, Torti SV. Iron and cancer: recent insights. *Ann N Y Acad Sci*. 2016;1368(1):149–61.
- Tang D, Chen X, Kang R, Kroemer G. Ferroptosis: molecular mechanisms and health implications. *Cell Res*. 2021;31(2):107–25.
- Liu J, Kang R, Tang D. Signaling pathways and defense mechanisms of ferroptosis. *Febs J*. 2022;289(22):7038–50.
- Chen M, Li X, Du B, Chen S, Li Y. Upstream stimulatory factor 2 inhibits erastin-induced ferroptosis in pancreatic cancer through transcriptional regulation of pyruvate kinase M2. *Biochem Pharmacol*. 2022;205:115255.
- Oh S, Shin S, Janknecht R. ETV1, 4 and 5: an oncogenic subfamily of ETS transcription factors. *Biochim Biophys Acta*. 2012;1826(1):1–12.
- Xu X, Wang B, Liu Y, Jing T, Xu G, Zhang L, et al. ETV4 potentiates nuclear YAP retention and activities to enhance the progression of hepatocellular carcinoma. *Cancer Lett*. 2022;537:215640.
- Singsuksawat E, Thuwajit C, Charngkaew K, Thuwajit P. Increased ETV4 expression correlates with estrogen-enhanced proliferation and invasiveness of cholangiocarcinoma cells. *Cancer Cell Int*. 2018;18:25.
- He R, Wei Y, Peng Z, Yang J, Zhou Z, Li A, et al.  $\alpha$ -Ketoglutarate alleviates osteoarthritis by inhibiting ferroptosis via the ETV4/SLC7A11/GPX4 signaling pathway. *Cell Mol Biol Lett*. 2024;29(1):88.
- Chen W, Song J, Liu S, Tang B, Shen L, Zhu J, et al. USP9X promotes apoptosis in cholangiocarcinoma by modulation expression of KIF1B $\beta$  via deubiquitinating EGLN3. *J Biomed Sci*. 2021;28(1):44.
- Zhao Y, Li M, Yao X, Fei Y, Lin Z, Li Z, et al. HCARI1/MCT1 regulates tumor ferroptosis through the Lactate-Mediated AMPK-SCD1 activity and its therapeutic implications. *Cell Rep*. 2020;33(10):108487.
- He Y, Yu X, Li J, Zhang Q, Zheng Q, Guo W. Role of m(5)C-related regulatory genes in the diagnosis and prognosis of hepatocellular carcinoma. *Am J Transl Res*. 2020;12(3):912–22.
- Liu J, Xiao S, Chen J, Lou W, Chen X. A comprehensive analysis for expression, diagnosis, and prognosis of m(5)C regulator in breast cancer and its ncRNA-mRNA regulatory mechanism. *Front Genet*. 2022;13:822721.
- Ding X, Zhang X, Fang P, Bai W. ETV4/NSUN2 axis modulates aerobic Glycolysis and malignancy in HSCC. *Hum Mol Genet*. 2024.
- Sirica AE, Gores GJ, Groopman JD, Selaru FM, Strazzabosco M, Wei Wang X, Zhu AX. Intrahepatic cholangiocarcinoma: continuing challenges and translational advances. *Hepatology*. 2019;69(4):1803–15.
- Huai H, Li J, Zhang X, Xu Q, Lan H. Creation of a rat Takotsubo syndrome model and utilization of machine learning algorithms for screening diagnostic biomarkers. *J Inflamm Res*. 2023;16:4833–43.
- Keld R, Guo B, Downey P, Gulmann C, Ang YS, Sharrocks AD. The ERK MAP kinase-PEA3/ETV4-MMP-1 axis is operative in oesophageal adenocarcinoma. *Mol Cancer*. 2010;9:313.
- Gao X, Jiang M, Chu Y, Han Y, Jin Y, Zhang W, et al. ETV4 promotes pancreatic ductal adenocarcinoma metastasis through activation of the CXCL13/CXCR5 signaling axis. *Cancer Lett*. 2022;524:42–56.

34. Cai LS, Chen QX, Fang SY, Lian MQ, Lian MJ, Cai MZ. ETV4 promotes the progression of gastric cancer through regulating KDM5D. *Eur Rev Med Pharmacol Sci.* 2020;24(5):2442–51.
35. Wu B, Liang Z, Lan H, Teng X, Wang C. The role of PKM2 in cancer progression and its structural and biological basis. *J Physiol Biochem.* 2024;80(2):261–75.
36. Yu W, Zeng F, Xiao Y, Chen L, Qu H, Hong J, et al. Targeting PKM2 improves the gemcitabine sensitivity of intrahepatic cholangiocarcinoma cells via inhibiting  $\beta$ -catenin signaling pathway. *Chem Biol Interact.* 2024;387:110816.
37. Qiao Q, Wang J, Liu S, Chang J, Zhou T, Li C, et al. USP28 promotes tumor progression and Glycolysis by stabilizing PKM2/Hif1- $\alpha$  in cholangiocarcinoma. *Cell Oncol (Dordr).* 2024;47(6):2217–31.
38. Zhao G, Yuan H, Li Q, Zhang J, Guo Y, Feng T, et al. DDX39B drives colorectal cancer progression by promoting the stability and nuclear translocation of PKM2. *Signal Transduct Target Ther.* 2022;7(1):275.
39. Ding X, Zhang X, Fang P, Bai W. ETV4/NSUN2 axis modulates aerobic Glycolysis and malignancy in HSCC. *Hum Mol Genet.* 2024;33(20):1729–47.
40. Liu F, Wang Q, Wang Z, Zhang S, Ni Q, Chang H. ETV4 promotes the progression of cholangiocarcinoma by regulating Glycolysis via the TGF- $\beta$  signaling. *Transl Oncol.* 2024;47:102035.
41. Zhu T, Zheng J, Zhuo W, Pan P, Li M, Zhang W, et al. ETV4 promotes breast cancer cell stemness by activating Glycolysis and CXCR4-mediated Sonic Hedgehog signaling. *Cell Death Discov.* 2021;7(1):126.
42. Zahra K, Dey T, Ashish, Mishra SP, Pandey U. Pyruvate kinase M2 and cancer: the role of PKM2 in promoting tumorigenesis. *Front Oncol.* 2020;10:159.
43. Toller-Kawahisa JE, Hiroki CH, Silva CMS, Nascimento DC, Públis GA, Martins TV, et al. The metabolic function of pyruvate kinase M2 regulates reactive oxygen species production and microbial killing by neutrophils. *Nat Commun.* 2023;14(1):4280.
44. Chen F, Liao J, Wu P, Cheng L, Ma Y, Zhang L, et al. Oridonin inhibits the occurrence and development of colorectal cancer by reversing the Warburg effect via reducing PKM2 dimer formation and preventing its entry into the nucleus. *Eur J Pharmacol.* 2023;954:175856.
45. Wang P, Hu Z, Yu S, Su S, Wu R, Chen C, et al. A novel protein encoded by circFOXP1 enhances ferroptosis and inhibits tumor recurrence in intrahepatic cholangiocarcinoma. *Cancer Lett.* 2024;598:217092.
46. Dixon SJ, Olzmann JA. The cell biology of ferroptosis. *Nat Rev Mol Cell Biol.* 2024;25(6):424–42.
47. Wang L, Zhang Y, Yang J, Liu L, Yao B, Tian Z, He J. The knockdown of ETV4 inhibits the papillary thyroid cancer development by promoting ferroptosis upon SLC7A11 downregulation. *DNA Cell Biol.* 2021;40(9):1211–21.
48. Ren C, Tan P, Gao L, Zeng Y, Hu S, Chen C, et al. Melatonin reduces radiation-induced ferroptosis in hippocampal neurons by activating the PKM2/NRF2/GPX4 signaling pathway. *Prog Neuropsychopharmacol Biol Psychiatry.* 2023;126:110777.
49. Li T, Huang HY, Qian B, Wang WH, Yuan Q, Zhang HY, et al. Intervening mitochondrial PD-L1 suppressed IFN- $\gamma$ -induced cancer stemness in hepatocellular carcinoma by sensitizing sorafenib-induced ferroptosis. *Free Radic Biol Med.* 2024;212:360–74.
50. Nagy Z, Seneviratne JA, Kanikevich M, Chang W, Mayoh C, Venkat P, et al. An ALYREF-MYCN coactivator complex drives neuroblastoma tumorigenesis through effects on USP3 and MYCN stability. *Nat Commun.* 2021;12(1):1881.
51. Zhou Z, Wu B, Chen J, Shen Y, Wang J, Chen X, et al. ETV4 facilitates proliferation, migration, and invasion of liver cancer by mediating TGF- $\beta$  signal transduction through activation of B3GNT3. *Genes Genomics.* 2023;45(11):1433–43.
52. Kwon OH, Kang TW, Kim JH, Kim M, Noh SM, Song KS, et al. Pyruvate kinase M2 promotes the growth of gastric cancer cells via regulation of Bcl-xL expression at transcriptional level. *Biochem Biophys Res Commun.* 2012;423(1):38–44.

#### Publisher's note

Springer Nature remains neutral with regard to jurisdictional claims in published maps and institutional affiliations.